Available online at www.sciencedirect.com
SCIENCE DIRECT
ELSEVIER
Icarus 178 (2005) 406–416
ICARUS
www.elsevier.com/locate/icarus

Diffuse auroral precipitation in the jovian upper atmosphere and magnetospheric electron flux variability

Bidushi Bhattacharya [a,*], Richard M. Thorne [b], Donald J. Williams [c], Krishan K. Khurana [d], Donald A. Gurnett [e]

[a] *Spitzer Science Center, Caltech, MS 220-6, 1200 E. California Blvd., Pasadena, CA 91125, USA*
[b] *Department of Atmospheric Sciences, UCLA, 7127 MS, Box 951565, 405 Hilgard Ave., Los Angeles, CA 90095, USA*
[c] *Applied Physics Laboratory, The Johns Hopkins University, 11100 Johns Hopkins Road, Laurel, MD 20723, USA*
[d] *Institute of Geophysics and Planetary Physics, UCLA, Box 951567, 405 Hilgard Ave., Los Angeles, CA 90095, USA*
[e] *Department of Physics and Astronomy, The University of Iowa, 203 Van Allen Hall, Iowa City, IA 52242, USA*

Received 20 September 2004; revised 29 April 2005

Available online 18 August 2005

Abstract

The deposition of energetic electrons in Jupiter's upper atmosphere provides a means, via auroral observations, of monitoring electron and plasma wave activity within the magnetosphere. Not only does particle precipitation indicate a potential change in atmospheric chemistry, it allows for the study of episodic, pronounced flux enhancements in the energetic electron population. A study has been made of the effects of such electron injections into the jovian magnetosphere and of their ability to provide the source population for variations in diffuse auroral emissions. To identify the source region of precipitating auroral electrons, we have investigated the pitch-angle distributions of high-resolution Galileo Energetic Particle Detector (EPD) data that indicate strong flux levels near the loss cone. The equatorial source region of precipitating electrons has been determined from the locations of Galileo's in situ measurements by tracing magnetic field lines using the KK97 model. The primary source region for Jupiter's diffuse aurora appears to lie in the magnetic equator at 15–40 R_J, with the predominant contribution to precipitation flux (tens of ergs $\mathrm{cm}^{-2}\,\mathrm{s}^{-1}\,\mathrm{sr}^{-1}$) stemming from <30 R_J. Variability of flux for energetic electrons in this region is also important to the irradiation of surfaces and atmospheres for the Galilean moons: Europa, Ganymede, and Callisto. The average diffuse auroral precipitation flux has been shown to vary by as much as a factor of six at a given radial location. This variability appears to be associated with electron injection events that have been identified in high-resolution Galileo EPD data. These electron flux enhancements are also associated with increased whistler-mode wave activity and magnetic field perturbations, as detected by the Galileo Plasma Wave Subsystem (PWS) and Magnetometer (MAG), respectively. Resonant interactions with the whistler-mode waves cause electron pitch-angle scattering and lead to pitch-angle isotropization and precipitation.

Keywords: Aurorae; Jupiter, atmosphere; Jupiter, magnetosphere

1. Introduction

The magnetospheric plasma sources at Earth and Jupiter are quite different, with terrestrial plasma primarily originating in the ionosphere or solar wind and jovian plasma stemming mainly from the satellite Io. In both systems, atmospheric precipitation leading to enhanced auroral emission serves as a marker for magnetospheric activity. In particular, substorm injections into the outer magnetosphere at Earth are associated with enhancement in auroral emission (e.g., Lyons, 1995). Within the jovian system, both spatial and temporal variability of energetic particle flux play a role in atmospheric and satellite processes. Mauk et al. (2002) have linked jovian auroral enhancements observed by the Hubble Space Telescope with Galileo EPD electron flux in-

* Corresponding author. Fax: +1 (626) 568 0673.
E-mail address: bhattach@ipac.caltech.edu (B. Bhattacharya).

0019-1035/$ – see front matter
doi:10.1016/j.icarus.2005.06.013

jections. EPD measurements near Ganymede indicate that while energetic electrons do have direct access to the moon's polar cap regions along field lines that are linked to Jupiter, the amount of power deposition is insufficient to trigger any measurable airglow or aurora-like phenomena (Paranicas et al., 1999). In addition, differential precipitation of energetic electrons across the surface of Europa and on Ganymede's polar caps leads to variations in radiolytic chemistry and has been associated with changes in optical albedo (Cooper et al., 2001; Paranicas et al., 2001).

The time-variability of energetic particle flux in the middle ($\sim 9 \leqslant R_J \leqslant 27$) jovian magnetosphere was discussed by Mauk et al. (1997, 1999), who identified energy-time dispersed enhancements of up to a factor of ten in the >20 keV electron population using low-resolution (real-time) in situ measurements by the Galileo EPD instrument (Williams et al., 1992). The episodic injection events appear to be associated with an interchange process that carries localized flux tubes with high phase space density in towards Jupiter. These events may also be related to small-scale interchange instabilities such as those identified within the Io torus (Bolton et al., 1997; Kivelson et al., 1997; Thorne et al., 1997) and in the vicinity of Europa's orbit (Russell et al., 2004).

The energy precipitation flux required to trigger Jupiter's diffuse aurora is predominantly supplied by energetic electrons from the middle magnetosphere. An initial study of Galileo EPD data (Bhattacharya et al., 2001) indicated that ion precipitation flux contributes less than a few erg $\mathrm{cm}^{-2}\,\mathrm{s}^{-1}$, which is an order of magnitude too weak to account for the diffuse aurora. In contrast, energetic electron precipitation, which is highly variable, typically exceeds a few tens of erg $\mathrm{cm}^{-2}\,\mathrm{s}^{-1}$ over a broad region in the middle magnetosphere (15–40 R_J). Quasi-isotropic electron pitch-angle distributions, indicative of scattering into the loss cone and subsequent precipitation, are always evident in the middle magnetosphere at >15 R_J; distributions in the inner magnetosphere ($R_J \leqslant 10$) are typically pancaked (peaked in the direction perpendicular to the magnetic field), with empty or nearly empty loss cones, leading to very little precipitation into the atmosphere.

During Galileo's first orbit through the inner jovian magnetosphere, Thorne et al. (1997), identified an isolated interchange event in which variations in particle flux were associated with enhanced plasma wave activity and changes in pitch-angle anisotropy. They noted a drop in the upper hybrid resonance line in Galileo PWS (Gurnett et al., 1992) measurements, indicative of a decrease in particle density. An associated study of similar events using observations from the Galileo MAG instrument (Kivelson et al. 1992, 1997) identified localized regions of enhanced magnetic field, which supported the concept of inward interchange transported in mass-depleted magnetic flux tubes. A third, related study by Bolton et al. (1997) using measurements from the PWS clearly identified the electromagnetic waves evident during this period to be whistlers that are capable of cyclotron resonance with electrons in the range 80 keV–5 MeV. This trio of papers makes a strong case for enhanced electron scattering into the loss cone via wave–particle interactions during injection events in the jovian magnetosphere.

Here, we address the origin of variations in electron energy precipitation flux from the middle jovian magnetosphere that were identified by Bhattacharya et al. (2001). To determine whether these variations are due to temporal changes in the magnetosphere or to spatial variability as the spacecraft moved away from the magnetic equator, the data were mapped to the equatorial source region. This was accomplished by field-line tracing using the KK97 (Khurana, 1997) magnetic field model (Section 2). Substantial variations in precipitation flux at a given L-shell still exist when observations are mapped to the magnetic equator, indicative of temporal variability. This motivated us to examine a set of electron injection events that have been identified in the available high-resolution EPD data. In Section 3, we present PWS and MAG observations that associate enhanced plasma wave activity and magnetic field disturbances with increases in energetic electron flux. Also in Section 3, we show that injection events are associated with pitch-angle isotropization and particle flux enhancements in the vicinity of the loss cone. We also look in detail at small-scale variations in the magnetic field and associated changes in electron density required to maintain magnetospheric pressure balance. The conditions for resonant interaction between the observed waves and energetic EPD electrons are addressed in Section 4, including a discussion of electron resonant energies, the required wave amplitudes for strong pitch-angle diffusion, and the anticipated pitch-angle distributions due to such wave–particle interactions.

2. Field-line tracing with the KK97 magnetic field model

2.1. Magnetic field model

In order to identify the source region for auroral particles, we have mapped EPD observations to the magnetic equatorial using the KK97 magnetic field model (Khurana, 1997). A planetary magnetic field can generally be expressed (Khurana, 1997) in terms of internal and external components B_i and B_e, attributed to currents in the central core of the planet or within the magnetosphere, respectively, as

$$\vec{B} = \vec{B}_i + \vec{B}_e. \tag{1}$$

The internal scalar potential V_i is usually expressed as a spherical harmonic expansion:

$$\vec{B}_i = -\vec{\nabla} V_i = a \sum_{n=0}^{n_{\max}} \left(\frac{a}{r}\right)^{n+1} \times \sum_{m=0}^{n} \left\{ P_n^m(\cos\theta)\left[g_n^m \cos(m\phi) + h_n^m \sin(m\phi)\right]\right\}, \tag{2}$$

where a is the planetary radius, and r is distance from the center of the planet, θ and ϕ are colatitude and longitude, P_m^n are Schmidt normalized Legendre functions of degree n and order m, and g_m^n and h_m^n are empirically determined Schmidt coefficients. The KK97 magnetic field model (Khurana, 1997) provides an expression for the external currents flowing in the equatorial current sheet and describes the internal component using Goddard Space Flight Center (GSFC) O6 model (Connerney, 1993), which assumes an octopolar field ($n = 3$) and computes a spherical harmonic expansion of V_i with coefficients derived empirically from Pioneer 11 and Voyager 1 observations. The KK97 model defines the equatorial current sheet in cylindrical coordinates in terms of scalar functions f and g,

$$\vec{B}_e = \vec{\nabla} f(r, \phi, Z) \times \vec{\nabla} g(r, \phi, Z), \tag{3}$$

where Z is height above the magnetic equator. The functions f and g are Euler potential functions that describe the external scalar potential and provide a realistic (e.g., non-infinite) value of the radial component of the field B_r at $r = 0$. These functions also account for the radial sweep-back of magnetic field lines away from Jupiter due to field-aligned and radial currents in the magnetosphere. The external component is empirically constrained by measurements from the Pioneer 10, Voyager 1, and Voyager 2 flybys. The KK97 model differs from a dipole at the surface of the planet due to higher order terms in the magnetic moment. In the magnetosphere, the addition of an external current sheet stretches field lines and gives a non-dipolar field that is clearly non-dipolar within a few R_J.

Field-line tracing is begun by computing (B_r, B_θ, B_φ) at a location where an EPD observation is available. From this point, an incremental step $\mathrm{d}\theta$ is taken and equations for the field-line

$$\frac{1}{r}\frac{\mathrm{d}r}{\mathrm{d}\theta} = \frac{B_r}{B_\theta} \quad \text{and} \quad \sin\theta \frac{\mathrm{d}\phi}{\mathrm{d}\theta} = \frac{B_\phi}{B_\theta} \tag{4}$$

are applied to determine the direction of the field. At the new position ($r + \mathrm{d}r$, $\theta + \mathrm{d}\theta$, $\varphi + \mathrm{d}\varphi$), the components of the field are again calculated. This process is repeated until the magnitude of the field $|\vec{B}| = (B_r^2 + B_\theta^2 + B_\varphi^2)^{1/2}$ reaches a minimum value. The position where this occurs is defined as the magnetic equator.

The Galileo spacecraft travels close to Jupiter's rotational equatorial plane, which is tilted from its magnetic equatorial plane by approximately 9°. This tilt results in motion of the spacecraft relative to the magnetic equator with a periodicity equal to the rotational period of the planet (~10 h). Note that the magnetic field is appreciably stretched out beyond 15 R_J. As Galileo moves in its trajectory away from the planet, the field becomes more distorted from a dipole, and small excursions from the magnetic equator at greater radial distances result in the spacecraft moving onto magnetic field lines that map to the distant, outer magnetosphere.

2.2. Precipitation energy flux

The field-line tracing method described above has been employed to map results presented by Bhattacharya et al. (2001) to the magnetic equator. We have also included record-mode observations from the G28 and G29 orbits, which were not available earlier, as well as all real-time observations at 15–40 R_J at the magnetic equator (as defined by local magnetic field minima). The relation for energy precipitation flux in Bhattacharya et al. (2001), Eq. (2), inadvertently contained a typographical error, although the calculations presented therein were performed correctly. The correct relation for energy precipitation flux ε in units of ergs cm^{-2} s^{-1} is provided here:

$$\varepsilon = \pi \int_{E_{k,\min}}^{E_{k,\max}} E_k j_p(E_k)\,\mathrm{d}E_k = \pi E_0^2 \int_{x_{\min}}^{x_{\max}} \frac{x J_0}{(x+1)^n}\,\mathrm{d}x, \tag{5}$$

where E_k is the kinetic energy of the particle in keV and $E_{k,\max}$, and $E_{k,\min}$ correspond to the maximum and minimum energies over which EPD data shows evidence of precipitation into the loss cone. The relation $j_p(E_k) = J_0/(1 + E_k/E_0)^n$ is a Lorentzian fit to the differential flux measured by EPD, J_0 and E_0 are scaling factors, and $x = E_k/E_0$, as described in Bhattacharya et al. (2001). Typical values for E_0 are 45–60 keV. $E_{k,\min} = 15$ keV in the majority of EPD observations, meaning the quasi-isotropic distributions are seen down to the lowest energies measurable by the instrument. The upper electron energy value for quasi-isotropy, $E_{k,\max}$, ranges from 188–527 keV and is not correlated with distance from the planet.

The electron precipitation flux calculated from Galileo data is shown in Fig. 1 as a function of magnetic equatorial crossing distance. Energy deposition of tens of ergs cm^{-2} s^{-1}, which is required to account for the diffuse auroral emission (Prangé et al., 1998), is evident from particles that originate in the region <40 R_J. Discrete auroral emission at Jupiter requires energy deposition that is ten times greater (Prangé et al., 1998), and we see no evidence of such a high level of energy precipitation in either the precipitating or the trapped particle distributions in the Galileo EPD data. Consequently, the discrete arcs in the main auroral oval must be due to particles that are accelerated by field-aligned potential drops close to Jupiter (e.g., Cowley and Bunce, 2001) that are associated with field-aligned current flow in the sub-corotational magnetosphere at 20–30 R_J (Kane et al., 1999).

It is assumed in this study that the energetic electron intensity measured outside the loss cone by EPD is comparable to that within the loss cone itself. The presence of electrons in the loss cone is attributed to resonant interactions with plasma waves, and whistler-mode waves in the appropriate frequency range to resonate with EPD electrons are identified in Fig. 3 below. As discussed in Section 4, in order for "strong pitch-angle diffusion" and a filled loss cone to occur, these whistlers must be intense enough to scatter a sufficient number of electrons. If strong diffusion is not present,

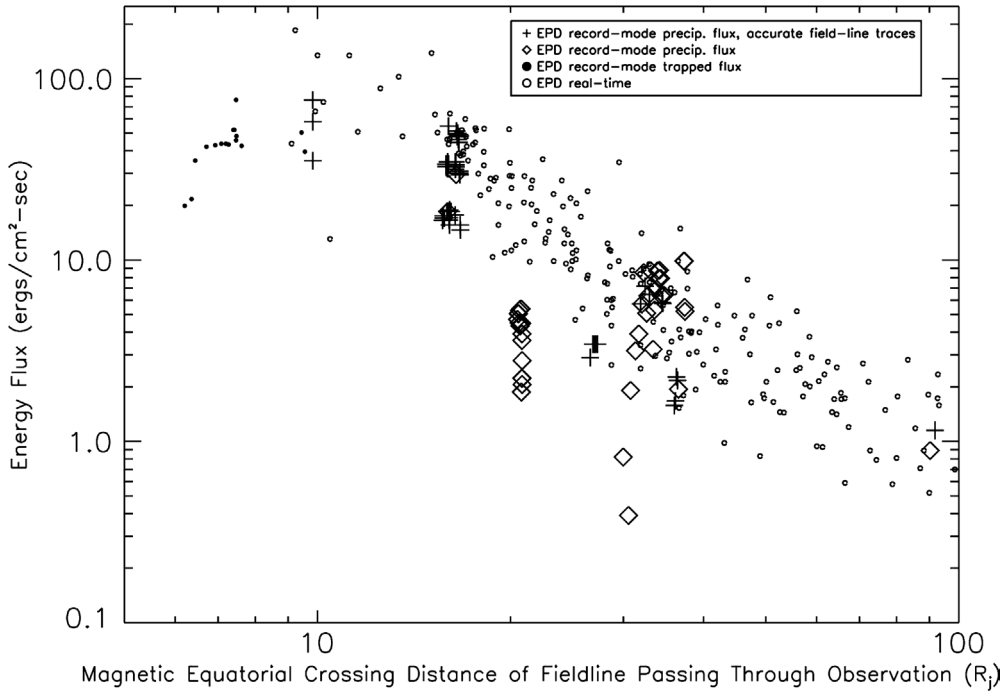

Fig. 1. Electron precipitation energy flux vs equatorial crossing point of magnetic field lines. Primary contribution to diffuse auroral emission in Jupiter's atmosphere comes from energetic electrons that originate in the magnetosphere at 15–40 R_J.

the precipitation flux values present here represent an upper limit.

While the KK97 model is considered accurate at all local times in the inner magnetosphere, it assumes azimuthal symmetry at all radial distances and consequently is only reliable on the nightside for the middle and outer magnetospheric regions (Khurana, 1997). EPD observations obtained from the dayside may therefore be less accurate in defining the origination point of precipitating electrons. We have compared magnetic field values predicted by the KK97 model to observations made by the Galileo (MAG). Energy flux calculations based on record-mode observations that are taken at locations where measured magnetic field values are within 10% of the KK97 model are identified by a "+" symbol in Fig. 1. Tracings at these locations more precisely identify the magnetic equator. The remaining record-mode observations are indicated with diamonds. Solid dots indicate trapped particle populations from the J0, C20, C22, and C23 record-mode datasets; these place an upper limit on precipitation flux in the inner magnetosphere. The open circles indicate energy fluxes derived from lower-resolution real-time data and represent a probable upper limit to precipitation flux, as distributions in the vicinity of the loss cone cannot be clearly identified in these data. The EPD is known to respond in a non-linear fashion to high counts, an issue that is currently being studied further by the instrument team. The EPD is likely to saturate at the lower energies (see Fig. 5 below), and the spectral distribution provided there may not fully provide a measure of the number of electrons present. Consequently, the higher precipitation flux values reported here represent a lower limit for the region 10–20 R_J, where particle count rates are highest.

Lower energy electrons measured by the Galileo Plasma Subsystem (PLS) have not been included in this study. Their contribution to diffuse auroral atmosphere may be significant, as the spectral distribution of electrons in the jovian magnetosphere indicates a higher prevalence of lower energy particles, as seen in Fig. 5. Paranicas et al. (1999) have extrapolated PLS and EPD data during the G2 and G7 encounters to estimate particle precipitation in the polar cap regions of Ganymede. Their findings make the case that deposition due to lower energy electrons is appreciable. As shown in their Fig. 8, PLS electrons at 0.1–3.0 keV deposit $\sim$0.5 ergs cm^{-2} s^{-1} of energy, which is just below 10% of the total energy contributed over the whole energy range by 0.1–100 keV electrons. While estimates of energy precipitation required to induce auroral emission at Ganymede have not been made, no detectable airglow has yet been reported (Paranicas et al., 1999).

To consider longitudinal location and its affect on precipitation flux, we have binned the high-resolution (record-mode) data as a function of local time. The number of precipitating distributions for each sector, as well as the median, minimum, and maximum energy flux for each orbit are summarized in Table 1. The statistics show that variation from the median is considerable, and the flux ratio ($E_{\text{precip,max}}/E_{\text{precip,min}}$) varies by at least a factor of two in six of 11 recordings (neglecting the G2 recording which has only one measurement). The available data do not evenly sample the jovian magnetosphere, and repeated observations are only available in the dawn and midnight sectors. It is

Table 1
Galileo EPD observations of precipitating electron pitch-angle distributions

Sector	Observation(s)* (YYYY:DOY)	(MLT)	Dist. (R_J)	No. of precip. dists	Energy precipitation flux (ergs cm^{-2} s^{-1})			
					Median	Max	Min	Max/min
Pre-dawn (0130–0430)	None	–	–	–	–	–	–	–
Dawn (0430–0730)	G8 recording (1997:126)	0600	25.2	25	6.4	8.8	0.4	22.54
	C9 encounter (1997:176)	0500	26.2	6	3.4	3.4	2.9	1.18
	C10 encounter (1997:259)	0500	26.1	9	2.3	9.9	1.6	6.25
	C23 encounter (1999:257)	0630	6.9	5	43.3	43.7	42.1	1.04
Morning (0730–1030)	G2 encounter (1996:250)	1045	15.2	1	29.6	29.6	29.6	1.00
	C20 recording (1999:123)	1000	9.4	3	50.4	76.3	39.5	1.93
	C22 recording (1999:224)	0830	7.4	5	48.2	52.1	42.6	1.22
Noon (1030–1330)	None	–	–	–	–	–	–	–
Afternoon (1330–1630)	E14 encounter (1999:088)	1430	9.6	3	57.8	76.2	35.4	2.16
Dusk (1630–1930)	C9 recording (1997:179)	1800	18.3	23	3.9	5.38	1.87	2.88
Evening (1930–2230)	None	–	–	–	–	–	–	–
Midnight (2230–0130)	G2 recording (1996:255)	2400	39	2	1.1	1.2	0.9	1.29
	G28 encounter (2000:141)	2400	15.0	50	33.7	54.8	14.6	3.74
	G29 encounter 2000:363	2200	15.4	14	18.5	18.9	18.5	1.02

* Observations designated as "encounter" were taken near a Galilean satellite, and those labeled as "recording" were taken along the trajectory towards or away from the moon.

not possible to draw conclusions about longitudinal variability with this dataset, as the radial distance of measurements at the dawn and midnight sectors differs considerably. Within these two regions, the precipitation flux from one encounter to the next, for the same radial distance, can vary appreciably. In the dawn sector at 25–26 R_J, the median flux ranges from 2.3 to 6.4 ergs cm^{-2} s^{-1}. In the midnight sector at 15 R_J, the median flux varies from 18.5 to 33.7 ergs cm^{-2} s^{-1}. Although the available EPD data are limited, measurements from these two sectors suggest that temporal variability does play an important role. In addition, changes in magnetic latitude of Galileo's position over time cannot account for the variations in energy precipitation that are observed at any given radial position. The lack of a clear relationship between location in the magnetosphere and energy flux has led us to examine temporal variation as a source of changes in precipitation flux. We discuss sudden increases in energetic electron flux in the section below.

3. Electron injection events

Not only can variability in electron flux in Jupiter's magnetosphere be linked to auroral phenomenon, it may be associated with observed variations in satellite albedo (Paranicas et al., 1999; Cooper et al., 2001). A greater presence of energetic electrons in the magnetosphere may lead to enhanced precipitation onto the moons, causing changes in surface chemistry and optical reflectivity (Cooper et al., 2001). We present in this section a summary of noted enhancements in Galileo EPD electron flux through the I32 encounter.

From a survey of all high-resolution (record-mode) EPD data, we have identified a series of electron injection events. Ten of the 32 record-mode datasets indicate sudden increases in energetic electron flux by factors of two to eight (Table 2). Some events show energy dispersion, which suggests that they occurred at a different jovigraphic longitude and that EPD detected the enhancements as particles gradient drifted to the position of the spacecraft (Mauk et al., 1997). Other injection events are evident in all EPD energy channels simultaneously, suggesting that they occurred close to the location of Galileo.

An example of electron flux enhancement observed during the C23 orbit (day 257 of 1999, 7.7–6.5 R_J) is shown in Fig. 2. There is a strong correlation between intensification of plasma waves (top panel) and the enhancement of energetic ($29 \leqslant E \leqslant 304$ keV) electron flux (bottom panel). EPD record-mode measurements begin at 14:36, when the injection event is already underway. Both electron flux and plasma wave intensities are anomalously high. Intense whistler-mode emission can be seen during this period extending up to ∼2 kHz. The solid white line near 20 kHz is the electron gyrofrequency. The lower band cutoff of the whistler-mode emissions is difficult to identify because of low frequency noise and possible Doppler broadening due the large velocity differential between the Galileo spacecraft and the plasma frame. At 15:06, a drop in 22–42 keV electron flux is immediately accompanied by diminished plasma wave activity. The next electron injection (15:10-15:16) is evident in both the 29–42 keV and 174–304 keV EPD channels and is accompanied by enhanced whistler-mode emission that cuts off near 2 kHz. During the period 15:16–15:44, Galileo returns to normal conditions found in the quiet-time background Io torus. Electron flux is reduced and exhibits a pronounced pancaked distribution, and whistler-mode waves are much weaker.

The record-mode pitch-angle measurements made in C23 are shown in Fig. 3. The background count rate due to penetrating particles that lie outside the measured energy range has been removed. Because of detector saturation issues, the distributions presented here indicate relative variations between different time periods, not changes in absolute count

Table 2
Galileo EPD record-mode observations of electron injection events

Orbit (YYDOY)	Dist. (R_J)	MLT	Injection period(s)	Energy range (keV)	Injection intensity (× nominal flux)	Energy/time dispersed?
J0 encounter	7.1	10.9	16:07–16:10	15–10,500	5	No
(95341)	6.7	11.2	16:37–16:40	15–10,500	5	No
	6.5	11.3	16:50–16:55	15–10,500	5	No
	6.3	11.5	17:07–17:15	15–10,500	5	No
C3 encounter	26.1	7.8	13:47–13:59	15–884	3	No
(96309)						
E6 encounter	9.5	12.9	16:47–16:49	15–188	3	No
(97051)	9.5	12.9	16:42–16:55	174–884	3	No
C10 mag. eq. rec.	9.2	1.1	23:06–23:12	15–188	2	No
(97261)						
E11 encounter	9.2	11.2	20:51–21:24	15–29	6	Yes
(97310)	9.2	11.2	20:51–21:24	29–42	6	Yes
	9.2	11.2	20:52–21:26	42–55	6	Yes
	9.2	11.2	20:57–21:24	55–93	4	Yes
	9.2	11.2	21:25–21:42	93–188	2	Yes
	9.2	11.2	21:26–21:35	15–188	3–5	No
C20 perijove rec.	9.0	10.0	16:08–16:10	15–93	3	Yes
(99123)	9.0	10.0	16:09–16:12	93–304	3	Yes
	9.2	10.1	16:09–16:37	15–55	3	Yes
	9.2	10.1	16:12–16:38	55–188	2	Yes
	9.0	10.1	16:14–16:17	174–527	2	Yes
	9.2	10.2	16:12–16:43	304–527	2	Yes
	9.4	10.2	16:38–16:46	15–55	2	Yes
	9.4	10.2	16:39–16:47	55–93	2	Yes
	9.4	10.2	16:32–16:46	174–188	2	Yes
	9.4	10.2	16:42–16:44	174–527	2	Yes
	9.4	10.3	16:48–16:51	42–304	1.2	Yes
	9.4	10.3	16:48–16:52	304–527	4	Yes
	9.4	10.7	16:49–17:00	527–884	4	Yes
	9.4	10.7	17:13–17:35	15–304	3–4	No
	9.4	10.7	17:38–17:52	15–304	2	No
C22 perijove rec.	7.3	9.9	11:10–11:16	15–527	1.3–5	–
(99224)*	7.3	10.3	11:50–11:53	15–527	1.3–5	–
	7.4	10.6	12:27–12:32	15–527	1.5–5	–
C23 perijove rec.	7.7	6.1	14:36–14:40	15–188	4	No
(99257)	7.6	6.2	14:42–14:50	15–527	4	No
	7.6	6.3	14:55–15:05	15–93	2	Yes
	7.5	6.3	14:52–15:12	93–527	3	Yes
	7.5	6.3	14:58–15:05	1500–10,500	3	Yes
	7.5	6.3	14:59–15:01	15–304	1.3	Yes
	7.5	6.4	15:10–15:14	304–884	2	Yes
	7.4	6.4	15:12–15:16	15–93	2	Yes
	7.4	6.4	15:15–15:17	93–188	2	Yes
	7.4	6.4	15:16–15:18	174–304	1.2	Yes
	7.4	6.4	15:17–15:19	304–527	1.5	Yes
	7.4	6.5	15:18–15:22	527–884	1.5	Yes
I27 encounter	5.9	7.4	11:40–11:52	15–29	2	Yes
(00053)	5.9	7.4	11:40–11:52	29–42	2	Yes
	5.9	7.4	11:40–11:57	42–55	2	Yes
	5.9	7.5	11:42–11:59	55–93	2	Yes
	5.9	7.5	11:43–12:00	93–188	2	Yes
	5.9	7.6	11:44–12:02	174–304	2	Yes
I32 encounter	8.3	23.3	16:10–16:52	15–527	2	No
(01288)	5.8	3.4	23:02–23:48	15–304	3	No

* Data taken in limited mode to protect EPD from intense radiation in vicinity of Io torus.

rate. For the two energy ranges shown here, the marked difference in electron distribution as a function of pitch-angle may be indicative of resonance with whistler-mode waves. During the initial injection at 14:37–14:44 (Fig. 3a), complex distributions are present. At 14:39, these distributions provide a signature of rapid variations in magnetic field

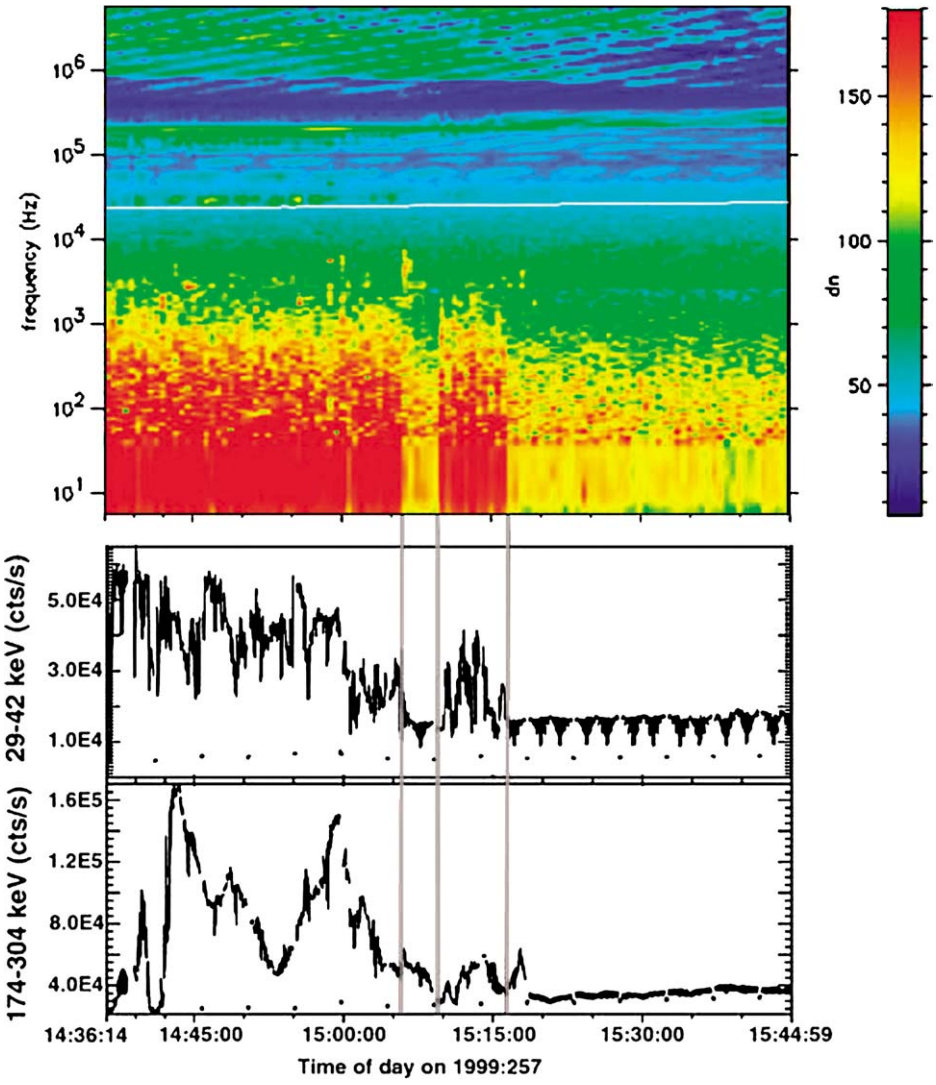

Fig. 2. Galileo PWS and EPD observations during an injection event during the C23 orbit. Electron enhancements are clearly associated with intensifications in plasma wave activity.

strength and electron flux that occurs during a spin period (19 s) of the Galileo spacecraft. A sharply varied pitch-angle distribution is evident at 14:39 as the spacecraft spins from 0°–180° relative to the magnetic field. Also evident is the development of butterfly distributions (extending to energies above 100 keV) at 14:39 and 14:42. These distributions could be evidence for a potential acceleration source region at higher latitudes, closer to the jovian atmosphere. Subsequent observations at 15:07 and 15:10 (Fig. 3b), when there is a reduction in plasma wave activity in Fig. 2, show weakly pancaked distributions. After the injection event has subsided at 15:26 (Fig. 3c), electron fluxes are substantially lower at all energies and pitch-angle distributions become pancake-shaped in the energy ranges shown.

The top four panels in Fig. 4 show Galileo MAG observations during the first set of injections discussed above. The spacecraft is moving closer to Jupiter, leading to an overall increase in the measured magnetic field strength. This general increase is superimposed on intermittent variations in the field. Although the overall magnetospheric dynamics at this location is governed by the large-scale electron injection, small-scale variations in electron flux also take place. Localized changes in the magnetic field, in response to variations in thermal pressure, are evident. A sudden rise in field strength from 14:40–14:42, where the radial component of the field drops, is associated with a drop in energetic electron flux, as shown in the bottom two panels of Fig. 4. Shorter periods of field enhancement are evident at 14:39 and 14:43, where the radial component of the magnetic field either decreases or does not change appreciably. There is a notable drop in 29–42 keV electron counts at 14:38, but the change in counts at 14:14 is less apparent.

Kivelson et al. (1997) have suggested that small-scale density depletions and associated magnetic field enhancements may be indicative of inward-moving flux tubes associated with interchange processes. To examine whether the data presented here are indicative of such a process, consider the time period 14:40–14:42 in Fig. 4. Energy spectra are

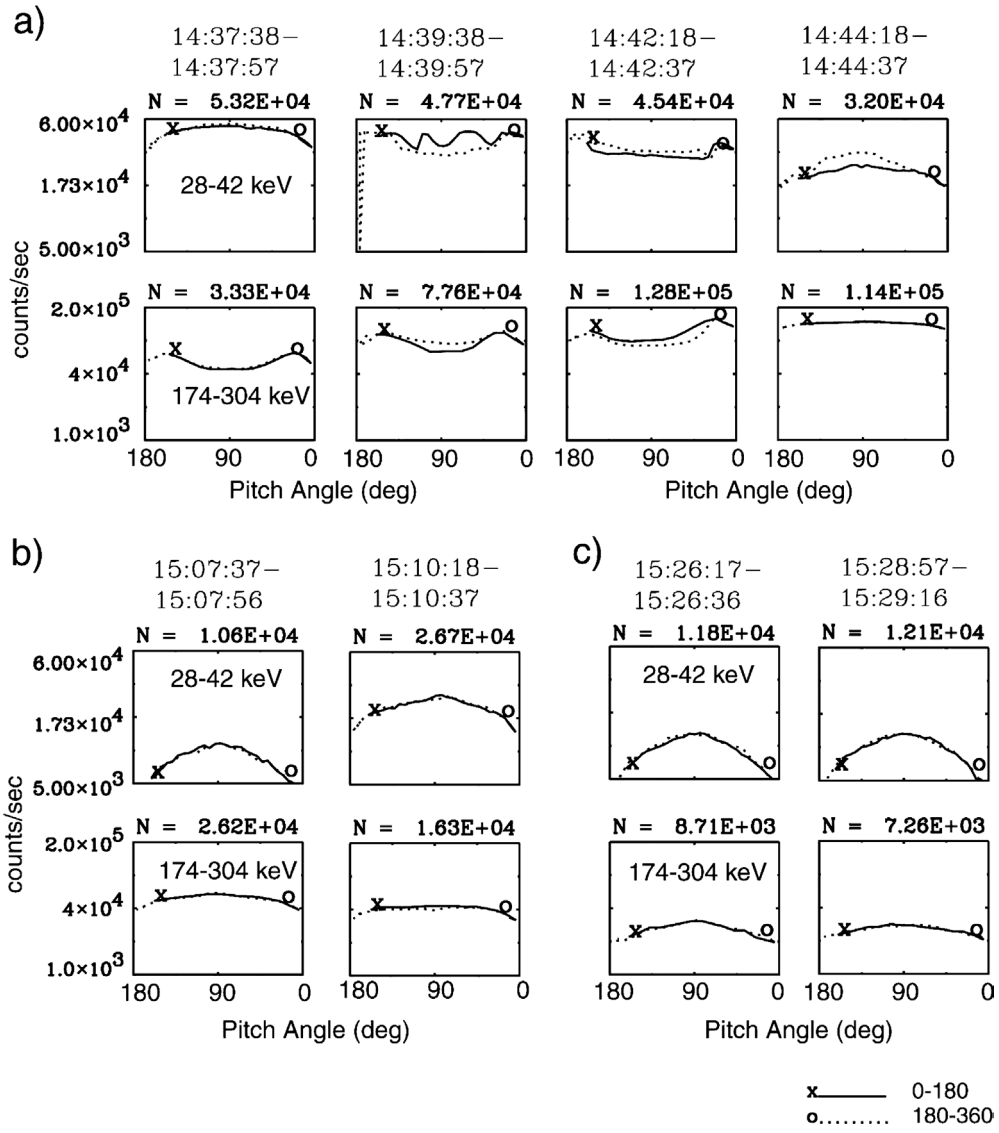

Fig. 3. Representative pitch-angle distributions during the C23 orbit. (a) During an injection, there is an enhancement in the vicinity of the loss cones, and short-term variations in magnetic field are evident. (b) In between injections, lower particle fluxes exhibit pronounced decreases, especially in the vicinity of the loss cone at lower energies. (c) During a quiet period in the background Io torus region, distributions are more pancaked.

provided for this period in Fig. 5. Spectra are shown before the magnetic field increase at 14:39:58, at the onset of field enhancement at 14:40:18, and during the period of maximum change in magnetic field at 14:40:38. At the highest energies, $E > 527$ keV, particle flux does not vary appreciably during the event. While electron flux at lower energies is comparable before and after the interchange, there is a noticeable drop at the onset of magnetic field change and an even sharper decrease in flux when the rate of increase of magnetic field is greatest.

Fig. 4 shows an intensification of $\Delta B = 20$ nT in field strength from 14:40–14:42. A change in magnetic pressure can be attributed to variations in plasma density, plasma temperature, or both. As a drop in the upper hybrid resonance line has been associated with previously studied interchange processes (Gurnett et al., 1992), we assume that magnetic pressure changes noted here can be attributed to primarily to density variations. To assess whether the associated increase in magnetic pressure is offset by a comparable decrease in thermal pressure of EPD electrons, consider

$$\Delta P_{\mathrm{mag}} = (\Delta B)^2/2\mu_0 \quad \text{and} \quad \Delta P_{\mathrm{th,EPD}} = \Delta n_{\mathrm{EPD}} kT. \qquad (6)$$

The number density above can be expressed in terms of particle flux and velocity, $\Delta n_{\mathrm{EPD}} \approx \Delta j_{\mathrm{EPD}}/v_{\mathrm{EPD}}$ for the relativistic EPD electrons. Fig. 5 shows the change in flux $\Delta j = 7.0 \times 10^6$ counts cm^{-2} s^{-1} for 29–42 keV electrons and $\Delta j = 3.50 \times 10^7$ counts cm^{-2} s^{-1} for 174–304 keV electrons, which are the two energy ranges presented in the bottom two panels in Fig. 4. The change in flux represented by EPD spectra in the lower energy range may be affected by detector saturation issues. If the counts measured are taken at face value, the total change in thermal

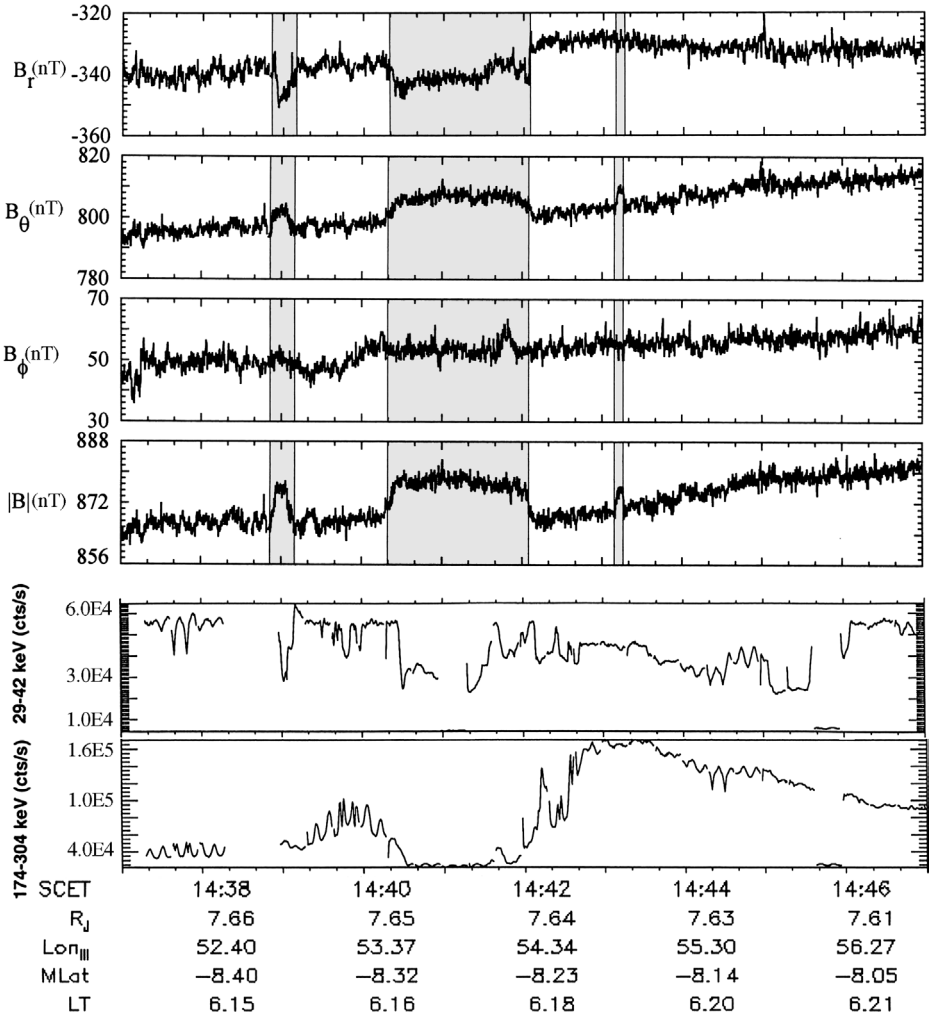

Fig. 4. Galileo MAG and EPD observations during an injection event during the C23 orbit. Increases in total magnetic field strength are associated with a drop in energetic electron counts.

pressure over the EPD range can be determined from the total change in energy density, $\Delta P_{\mathrm{th,EPD}} = 1.71 \times 10^{-11}$ Pa. This can be compared to the total change in magnetic pressure, $\Delta P_{\mathrm{mag}} = 1.59 \times 10^{-10}$ Pa. The EPD electron population by itself may not supply a sufficient density depletion to offset the observed ΔP_{mag}. EPD ion data during this time do not demonstrate any variation in flux and consequently do not contribute to the thermal pressure variation. Lower energy particles, measured by the Galileo PLS, may also contribute to the total drop in particle pressure, and these data need to be included to gain a complete understanding of the role of electron depletion in interchange events.

4. Wave–particle interactions

The large variability in precipitation energy flux at fixed radial locations (Fig. 1) could either be an indication of varying degrees of pitch-angle scattering into the loss cone or of increased flux due to injections. If energetic electrons are supplied to the Io torus by inward radial transport while conserving the first two adiabatic invariants, their pitch-angle distributions are expected to become pancake-shaped. The distributions in Fig. 3a clearly provide evidence to the contrary during injection events.

Violation of the first two adiabatic invariants can occur when particles are subject to force fields that vary on timescales shorter than the particle gyroperiod or bounce period (e.g., Schulz and Lanzerotti, 1974). A variety of processes contribute to the non-adiabatic behavior in the jovian magnetosphere. Current sheet scattering (Birmingham, 1984) due to field-line curvature comparable to electron Larmor radius, can occur in the outer magnetosphere ($>30\ R_J$), where magnetic field-lines are substantially distorted (Khurana, 1997). In the middle and inner magnetosphere ($<30\ R_J$), which maps to the auroral zone, the magnetic field is less distorted, and pitch-angle scattering can occur during resonant interactions with plasma waves (e.g., Thorne, 1983). Such scattering can rapidly modify electron pitch-angle distributions during an injection event, when the waves are enhanced (Fig. 3).

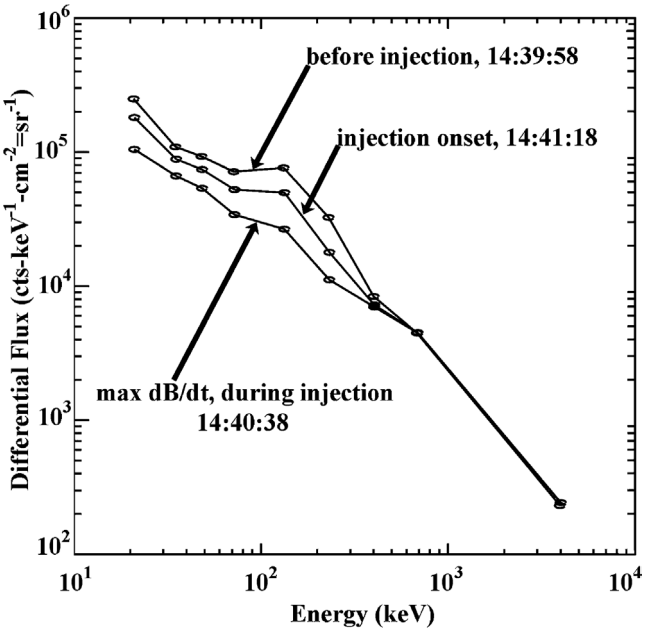

Fig. 5. Galileo EPD electron energy spectra before an injection, at the onset of an injection, and at maximum $\mathrm{d}B/\mathrm{d}t$. In all but the two highest energy channels, fluxes change by approximately a factor of two. It should be noted that the EPD does not respond in a linear fashion in the lower energy channels shown here, and the "scooped out" appearance of the spectra may be in part due to saturation effects.

Plasma waves may be excited by sudden injections of energetic plasma during interchange interactions such as those described by Bolton et al. (1997), Kivelson et al. (1997), and Thorne et al. (1997). During an interchange event, mass-loaded magnetic flux tubes containing iogenic, thermal plasma are centrifugally driven outwards and are replaced by inward-flowing, mass-depleted magnetic flux tubes that contain adiabatically energized plasma. The rapid influx of anisotropic, energetic electrons provides a source of free energy for the generation of observed whistler-mode waves (e.g., Bolton et al., 1997). Gyroresonant interactions between electrons and whistler-mode waves occur when

$$\omega - k_{\|} v_{\|} = \frac{\Omega_-}{\gamma}, \tag{7}$$

where ω is the wave frequency, $k_{\|}$ and $v_{\|}$ are the wave number and parallel velocity, Ω_- ($=\mathrm{qB\,mc^{-1}}$) is electron gyrofrequency, and $\gamma = (1 - v^2/c^2)^{-1/2}$ is the relativistic mass enhancement factor. The relativistic resonance condition defines an ellipse in velocity space (e.g., Xiao et al., 1998). Using the standard dispersion relation for low frequency ($\omega/\Omega_- \ll 1$), field-aligned whistler-mode emissions, one may solve (7) for the minimum resonant electron energy (which occurs when $v_\perp = 0$). Over the upper portion of the whistler-mode wave band ($0.01 \leqslant \omega/\Omega_- \leqslant 0.1$) shown in Fig. 2, the minimum resonant electron energy lies between 383 and 46 keV, assuming $\omega_p/\Omega_- \sim 7$. These whistler-mode waves are therefore able to resonate with the electrons detected by EPD. As long as the waves are of sufficient amplitude to lead to "strong pitch-angle diffusion," resultant scattering could be responsible for the quasi-isotropic distributions seen during the injection event (Fig. 3). The degree of isotropization at different energies in this figure may be indicative of waves that resonate with particles of a particular energy range. For a dipolar magnetic field, the wave amplitude required for strong diffusion scattering is proportional to $L^{-7/2}$ (Thorne, 1983). At 7.6 R_J, this corresponds to wave amplitudes of $B'_{\mathrm{SD}} \sim 65.5$ pT for 100 keV electrons. At larger radial distances, the required wave amplitude for strong pitch angle scattering falls off rapidly, and relatively modest wave intensities may be sufficient to induce quasi-isotropic pitch-angle distributions in the middle magnetosphere ($B'_{\mathrm{SD}} \leqslant 6.2$ pT, $L \geqslant 15$), which maps to the main auroral region at Jupiter.

5. Concluding remarks

By tracing field lines to the magnetic equator, we have established the source region of auroral electrons measured by Galileo's EPD. Quasi-isotropic distributions observed at different magnetic latitudes appear to originate in the middle magnetosphere at 15–40 R_J. There is appreciable variability in precipitation flux, which can be related to temporal changes in the energetic electron particle population. While longitudinal variations of electron flux cannot be ruled out in the dataset presented here, temporal variations at a given location are clearly evident. There is a strong correlation between periods of enhanced electron flux and increased whistler-mode wave activity. The intensification of waves can also be associated with pitch-angle isotropization. In addition, we have identified small-scale magnetic field disturbances that are associated with the inward transport of mass-depleted magnetic flux tubes as part of the interchange transport process. The change in plasma density required to offset measured field disturbances may not be supplied by electrons in the 15 keV–10.5 MeV energy range alone.

Although the injection event presented here is measured in the extended torus region, it may originate in the outer magnetosphere (e.g., Thorne et al., 1997). Magnetospheric electrons are known to be responsible for surface chemistry processes on Europa, Ganymede, and Callisto (Paranicas et al., 1999; Cooper et al., 2001). Injections may also play a role in variations of optical reflectance on the surfaces of Europa and Ganymede (Cooper et al., 2001). Jupiter's diffuse aurora may be the result of magnetospheric processes that are related to the pitch-angle anisotropies associated with electron injection events. The injection events trigger the generation of plasma waves, which in turn resonate with ambient electrons. Resonant interactions lead to pitch-angle scattering and enhanced atmospheric precipitation. We are thus able to associate electron injections in the jovian magnetosphere with increased diffuse auroral emissivity. The appearance of field-aligned distributions during injections could be a signature of field-aligned currents that flow in response to the injection events.

In the future, we plan to quantify the rate of electron pitch-angle scattering to determine if strong diffusion occurs in the jovian magnetosphere's auroral zone. We will examine in detail the effects of Doppler broadening on the lower frequency waves measured by PWS as well as the dispersive properties of waves during EPD electron injection events. Specifically, we plan to determine if the measured waves are capable of inducing strong pitch-angle scattering, thus leading to the observed isotropic electron distributions that are responsible for diffuse auroral emission in Jupiter's upper atmosphere.

Acknowledgments

This research was conducted under NASA Grant NAG5-11216. Support for this work was also provided by a NASA Grant to JPL/Caltech and under the auspices of the Spitzer Science Center. The authors wish to thank Dr. Jay Ansher for providing plasma density values and Dr. Eftyhia Zesta for providing assistance in development of the field-line mapping algorithm. Dr. Margaret Kivelson, PI for the Galileo Magnetometer, provided MAG data and useful comments.

References

Bhattacharya, B., Thorne, R.M., Williams, D.J., 2001. On the energy source for diffuse jovian auroral emissivity. Geophys. Res. Lett. 28, 2751–2754.

Birmingham, T.J., 1984. Pitch angle diffusion in the jovian magnetodisc. J. Geophys. Res. 89, 2699–2707.

Bolton, S.J., Thorne, R.M., Gurnett, D.A., Kurth, W.S., Williams, D.J., 1997. Enhanced whistler-mode emissions: Signatures of interchange motion in the Io torus. Geophys. Res. Lett. 24, 2123.

Connerney, J.E.P., 1993. Magnetic fields of the outer planets. J. Geophys. Res. 98, 18659–18679.

Cooper, J.F., Johnson, R.E., Mauk, B.H., Garrett, H.B., Gehrels, N., 2001. Energetic ion and electron irradiation of the icy Galilean satellites. Icarus 149, 133–159.

Cowley, S.W.H., Bunce, E.J., 2001. Origin of the main auroral oval in Jupiter's coupled magnetosphere–ionosphere system. Planet. Space Sci. 49, 1067–1088.

Gurnett, D.A., Kurth, W.S., Shaw, R.R., Roux, A., Gendrin, R., Kennel, C.F., Scarf, F.L., Shawhan, S.D., 1992. The Galileo plasma wave investigation. Space Sci. Rev. 60, 341–355.

Kane, M., Williams, D.J., Mauk, B.H., McEntire, R.W., Roelof, E.C., 1999. Galileo energetic particle detector measurements of hot ions in the neutral sheet region of Jupiter's magnetodisk. Geophys. Res. Lett. 26, 5–8.

Khurana, K.K., 1997. Euler potential models of the Jupiter's magnetospheric field. J. Geophys. Res. 102, 11295–11306.

Kivelson, M.G., Khurana, K.K., Means, J.D., Russell, C.T., Snare, R.C., 1992. The Galileo magnetic field investigation. Space Sci. Rev. 60, 357–383.

Kivelson, M.G., Khurana, K.K., Russell, C.T., Walker, R.J., 1997. Intermittent short-duration magnetic field anomalies in the Io torus: Evidence for plasma interchange? Geophys. Res. Lett. 24, 2127–2130.

Lyons, L.R., 1995. A new theory for magnetospheric substorms. J. Geophys. Res. 100, 19069–19081.

Mauk, B.H., Williams, D.J., McEntire, R.W., 1997. Energy-time dispersed charged particle signatures of dynamic injections in Jupiter's inner magnetosphere. Geophys. Res. Lett. 24, 2949–2952.

Mauk, B.H., Williams, D.J., McEntire, R.W., Khurana, K.K., Roederer, J.G., 1999. Storm-like dynamics of Jupiter's inner and middle magnetosphere. J. Geophys. Res. 104, 22759–22778.

Mauk, B.H., Clarke, J.T., Grodent, D., Waite Jr., J.H., Paranicas, C.P., Williams, D.J., 2002. Transient aurora on Jupiter from injections of magnetospheric electrons. Nature 415, 1003–1005.

Paranicas, C., Paterson, W.R., Cheng, A.F., Maun, B.H., McEntire, R.W., Frank, L.A., Williams, D.J., 1999. Energetic particle observations near Ganymede. J. Geophys. Res. 104, 17459–17470.

Paranicas, C., Carlson, R.W., Johnson, R.E., 2001. Electron bombardment of Europa. Geophys. Res. Lett. 28, 673–676.

Prangé, R., Rego, D., Pallier, L., Connerney, J., Zarka, P., Queinnec, J., 1998. Detailed study of FUV jovian auroral features with the post-COSTAR HST Faint Object Camera. J. Geophys. Res. 103, 20195–20216.

Russell, C.T., Georgilas, S., Mauk, B.H., Williams, D.J., 2004. Io as the trigger of energetic electron disturbances in the inner jovian magnetosphere. Adv. Space Res. 34, 2242–2246.

Schulz, M., Lanzerotti, L.J., 1974. Particle Diffusion in the Radiation Belts. Springer-Verlag, Heidelberg.

Thorne, R.M., 1983. Microscopic plasma processes. In: Dessler, A.J. (Ed.), Physics of the Jovian Magnetosphere. Cambridge Univ. Press, New York, pp. 454–488.

Thorne, R.M., Bolton, S.J., Armstrong, T.P., Gurnett, D.A., Kivelson, M.G., McEntire, R.W., Williams, D.J., 1997. Galileo evidence for rapid interchange transport in the Io torus. Geophys. Res. Lett. 24, 2131.

Williams, D.J., McEntire, R.W., Jaskulek, S., Wilken, B., 1992. The Galileo energetic particles detector. Space Sci. Rev. 60, 385–412.

Xiao, F., Thorne, R.M., Summers, D., 1998. Instability of electromagnetic R-mode waves in a relativistic plasma. Phys. Plasmas 5, 2489–2497.